Received: 29 March 2022 | Revised: 10 November 2022 | Accepted: 10 November 2022

DOI: 10.1002/mp.16121

RESEARCH ARTICLE

MEDICAL PHYSICS

Enhanced Cherenkov imaging for real-time beam visualization by applying a novel carbon quantum dot sheeting in radiotherapy

Xing Di[1] | **Changran Geng**[1,2] | **Chang Guo**[3] | **Yufen Shang**[4] | **Hongtao Fu**[4] | **Haonan Han**[1] | **Xiaobin Tang**[1,2]

[1]Department of Nuclear Science and Technology, Nanjing University of Aeronautics and Astronautics, Nanjing, People's Republic of China

[2]Joint International Research Laboratory on Advanced Particle Therapy, Nanjing University of Aeronautics and Astronautics, Nanjing, People's Republic of China

[3]Department of Radiation Oncology, Jiangsu Cancer Hospital, Nanjing, People's Republic of China

[4]Department of Radiation Physics, Dezhou Second People's Hospital, Dezhou, People's Republic of China

Correspondence
Changran Geng, Department of Nuclear Science and Technology, Nanjing University of Aeronautics and Astronautics, Nanjing 210016, People's Republic of China
Email: gengchr@nuaa.edu.cn

Di X, Geng C, Guo C, et al. Enhanced Cherenkov imaging for real-time beam visualization by applying a novel carbon quantum dot sheeting in radiotherapy. *Med Phys*. 2022;00:00-00.

Funding information
National Natural Science Foundation of China, Grant/Award Numbers: 12005102, 12075120; Foundation of Graduate Innovation Center in NUAA, Grant/Award Number: xcxjh20210623; Natural Science Foundation of Jiangsu Province, Grant/Award Number: BK20220132; Primary Research and Development Plan of Jiangsu Province, Grant/Award Number: BE2019002-3

Background: Cherenkov imaging can be used to visualize the placement of the beam directly on the patient's surface tissue and evaluate the accuracy of treatment planning. However, Cherenkov emission intensity is lower than ambient light. At present, time gating is the only way to realize Cherenkov imaging with ambient light.

Purpose: This study proposes preparing a novel carbon quantum dot (cQD) sheeting to adjust the wavelength of Cherenkov emission to obtain the optimal wavelength meeting the sensitive detection region of the camera, meanwhile the total optical signal is also increased. By combining a specific filter, this approach might help in using lower-cost camera systems without intensifier-coupled to accomplish in vivo monitoring of the surface beam profile on patients with ambient light.

Methods: The cQD sheetings were prepared by spin coating and UV curing with different concentrations. All experiments were performed on the Varian VitalBeam system and optical emission was captured using an electron multiplying charge-coupled device (EMCCD) camera. To quantify the optical characteristics and certify the improvement of light intensity as well as signal-to-noise ratio (SNR) of cQD sheeting, the first part of the study was carried out on solid water with 6 and 10 MV photon beams. The second part was carried out on an anthropomorphic phantom to explore the applicability of sheeting when using different radiotherapy materials and the imaging effect of sheeting with the impact of ambient light sources. Additionally, thanks to the narrow emission spectrum of the cQD, a band-pass filter was tested to reduce the effect from environmental lights.

Results: The experimental results show that the optical intensity collected with sheeting has an excellent linear relationship ($R^2 > 0.99$) with the dose for 6 and 10 MV photons. The full-width half maximum (FWHM) in x and y axis matched with the measured EBT film image, with accuracy in the range of ± 1.2 and ± 2.7 mm standard deviation, respectively. CQD sheeting can significantly improve the light intensity and SNR of optical images. Using 0.1 mg/ml sheeting as an example, the signal intensity is increased by 209%, and the SNR is increased by 147.71% at 6 MV photons. The imaging on the anthropomorphic phantom verified that cQD sheeting could be applied to different radiotherapy materials. The average optical intensity increased by about 69.25%, 63.72%, and 61.78%, respectively, after adding cQD sheeting to bolus, mask sample and the combination of bolus and mask. Corresponding SNR is improved by about 62.78%, 56.77%, and 68.80%, respectively. Through the sheeting, optical images with SNR > 5 can be obtained in the presence of ambient light and it can be

improved through combining with a band-pass filter. When red ambient lights are on, the SNR is increased by about 98.85% after adding a specific filter.
Conclusion: Through a combination of cQD sheeting and corresponding filter, light intensity and SNR of optical images can be increased significantly, and it shed new light on the promotion of the clinical application of optical imaging to visualize the beam in radiotherapy.

KEYWORDS
carbon quantum dot, Cherenkov, optical imaging, real-time beam visualization

1 | INTRODUCTION

As one of the three main approaches to treating malignant tumors, radiotherapy has the advantages of broad applicability, flexibility, and the ability to preserve organ function.[1,2] The outcome of radiotherapy depends on the accuracy of radiation dose delivery. However, due to patient movement, anatomical variations and uncertainties of treatment delivery parameters, erroneous dose can be delivered which can result in patient injury.[3] TLD and OSLD have been widely used in point dose measurement, however, they do not have online verification capacity due to the need for time-intensive readout processing.[4,5] Electronic portal imaging device (EPID) has also made great advancement in recent years. This technique allows real-time monitoring of radiation fluence and new techniques have been developed to reconstruct the dose delivered to a patient at each fraction.[6] The dosimetry systems based on EPID have difficulties in obtaining surface dose information and it has a large amount of patient scatters during measurement. Nowadays, with the extensive application of Cherenkov light, real-time beam visualization is developing rapidly, it can be used to evaluate the accuracy irradiation position.

Cherenkov photons with a spectrum of 300−800 nm can be emitted when a charged particle traverses a dielectric medium faster than the phase velocity of light in the given medium.[7] Previous studies have indicated that the Cherenkov signal intensity is linearly correlated with the dose delivered to the medium.[8–10] Based on this relationship, some studies have been conducted to evaluate the surface dose distribution on the skin in breast treatment,[11,12] head and neck treatment,[13] and total body electron treatment,[14,15] as the verification of the treatment plan. Compared with conventional methods of dose measurement, this optical imaging has the advantages of high spatial resolution, high sensitivity, and fast imaging speed. However, the emitted Cherenkov photons are scattered and absorbed by tissues, especially for dark tissues with high absorption coefficients, with the result that the Cherenkov signal is difficult to be collected by CCD. For Cherenkov imaging in radiotherapy, there have been studies on how to improve the detection efficiency of Cherenkov emission to acquire high signal-to-noise ratio (SNR) and image quality.[16] Zhang et al. proposed a method to suppress the influence of ambient light by gating the camera to obtain images only during x-ray pulses and subtracting the background image in between pulses.[17,18] However, in order to ensure that imaging cameras can collect light only during a delivery of a radiation pulse by the linac, intensified CMOS/CCD camera is usually used for image acquisition. This greatly increases the cost of the method. Meanwhile, although the time structure can be utilized for background subtraction,[19] however, this may not be possible with continuous irradiation sources such as those in Co-60 Gamma Knife or proton systems based on isochronous cyclotron.

In this study, we propose a method to improve the quality of optical imaging by using a novel carbon quantum dots (cQD) sheeting to achieve optimal wavelength meeting the sensitive detection region of the camera and increase the total optical signal without using an intensified camera system. With the use of cQD sheeting, the optical emission is composed of three parts: Cherenkov photons generated in the superficial surface of the tissue, the fluorescence excited by the Cherenkov photons, and the radioluminescence generated in cQD (Figure 2a and b). The luminescence uniformity, stability, and dose-response of the cQD sheeting are characterized through optical imaging. Different radiotherapy materials are used to observe the influence of cQD sheeting on the quality of the detected signal. Considering the requirements of patients for the room light source during the treatment, finally, LED with specific spectra is used as ambient light sources to explore the optical imaging effect of cQD sheeting under the existence of ambient light, and the band-pass filter is used to reduce the effect from the environmental lights.

2 | METHODS AND MATERIALS

2.1 | Preparation of the cQD sheeting

Carbon quantum dot is a carbon-based, zero-dimensional material with excellent biocompatibility, and its absorption spectra is consistent with the Cherenkov emission spectra.[20] Absorption and emission spectra

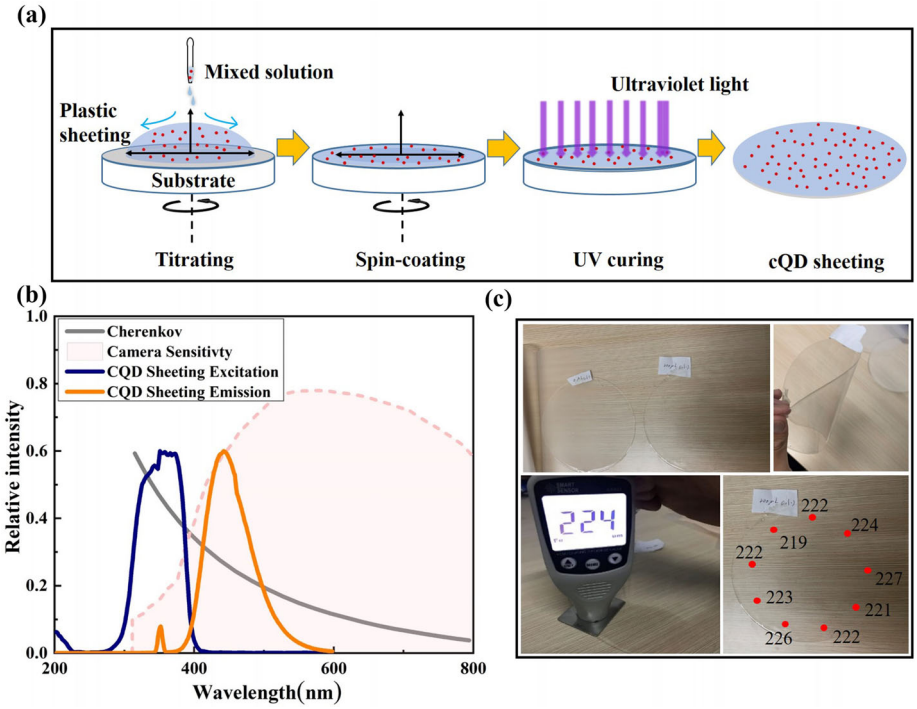

FIGURE 1 (a) Schematic diagram of cQD sheeting preparation process. (b) The Cherenkov spectrum (grey), the absorption spectra (blue), and the luminescence emission spectra (orange) of the cQD sheeting, the shaded area is the wavelength-dependent relative camera sensitivity. (c) Samples of cQD sheeting and schematic of its flexibility and thickness

of cQD has a minimal overlap, which results in reduced optical blurring caused by re-absorption.

The mean diameter of cQDs (produced by Suzhou Xingshuo Nanotechnology) used in this study is 10 nm. The cQD solution and UV-curable adhesive (made by Hefei Jingcheng Technology), which is liquid at room temperature and pressure, are evenly mixed at a certain volume ratio at a temperature of 30°C in a magnetic mixer. A substrate (polymethyl methacrylate) coated with plastic sheeting is horizontally fixed on the tray of a rotary coater through a vacuum pump. And then the solution is dropped on the rotating plastic sheeting through the dropper. Under the action of centrifugal force generated by the rotation of the rotary coating machine, the solution smoothly and evenly spreads on the surface of plastic sheeting. Finally, the sheeting is solidified with an ultraviolet lamp of 365–400 nm wavelength and an irradiation intensity of 10 Mw/cm^2 for 40 s. Given the light transmittance of sheeting, the cQD sheeting is prepared with concentrations of 0, 0.05, and 0.1 mg/ml, respectively. Among them, 0 mg/ml sheeting is the control group which means cQD free and completely prepared by UV curing adhesive. Figure 1a shows the schematic diagram of the sheeting preparation process.

The absorption and emission spectra of the cQD sheeting are measured by a fluorescence spectrophotometer (Cary Eclipse, Agilent Technologies G9800a, Malaysia, measurement range 200–900 nm, 1 nm scanning accuracy), as shown in Figure 1b. The thickness of cQD sheeting is within the range of 222 ± 5 μm with a diameter of 15 cm measured by a coating thickness gauge (measurement range 0–1700 μm, 1 μm measurement accuracy). CQD sheeting also has high flexibility to ensure it can be fitted on the patient's surface (Figure 1c).

2.2 | Experimental radiation delivery

This study is performed on the VitalBeam system (Varian Medical Systems). To quantify the optical characteristics and certify the improvement of light intensity as well as SNR of cQD sheeting, the first part of the study is carried out on the solid water. The second part is carried out on the anthropomorphous phantom to explore the applicability of cQD sheeting when using different radiotherapy materials and the imaging effect of cQD sheeting with the impact of ambient light sources. The diagram of the experiments is illustrated in Figures 2e and f. To suppress the influence of ambient light on light detection, the indoor lighting is turned off before image acquisition except in the research of imaging effect with ambient light.

In the first part, the solid water is covered with a 2 mm layer of uniform, light colored skin-toned clay (SuperSculpey Original) to mimic the optical properties of skin. Ahmed et al. have validated the tissue-like optical properties of the used modeling clay by measuring its

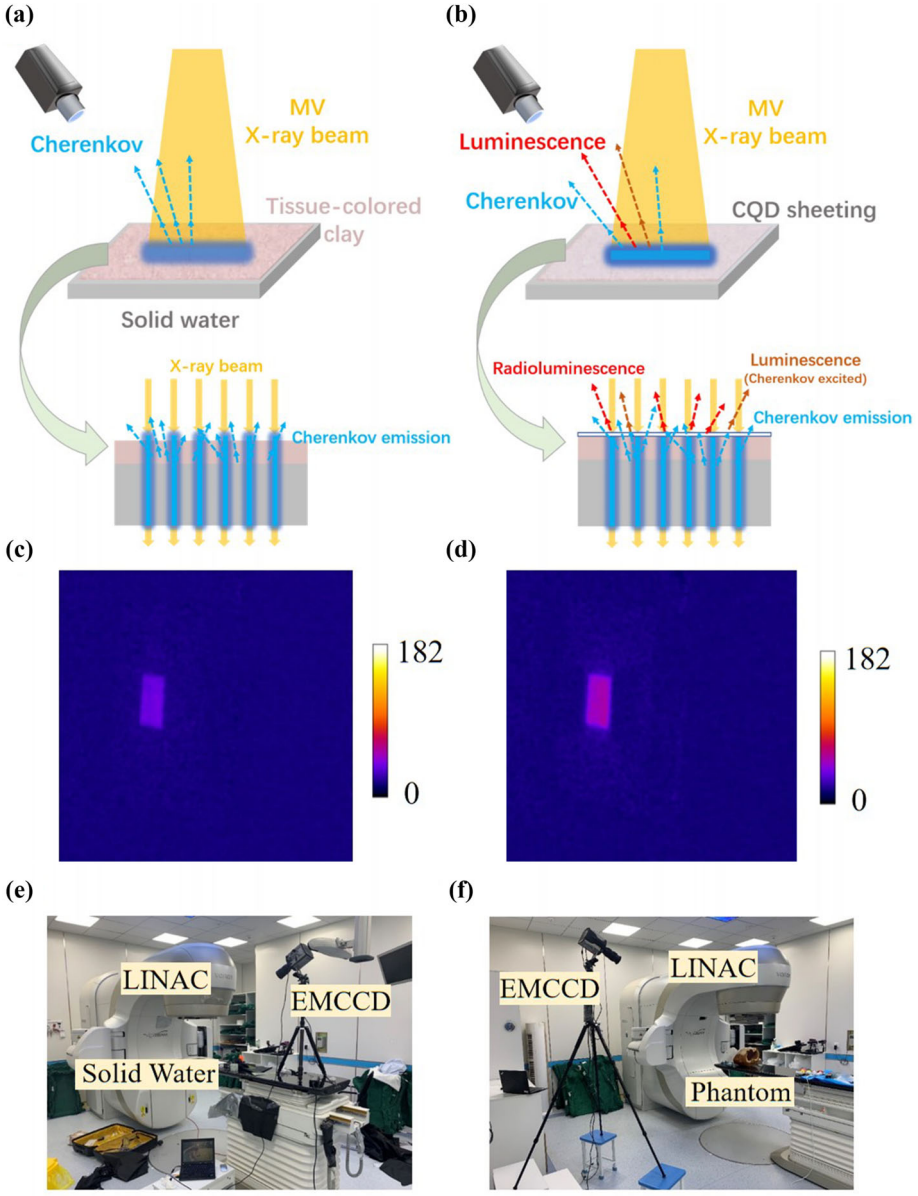

FIGURE 2 Schematic of the luminescence emission without sheeting (a) and with the cQD sheeting (b). (c) Single-frame image of luminescence from a broad solid water without sheeting. (d) Corresponding image with cQD sheeting on. (e, f) Photographs of solid water and phantom imaging setup

absorption and scattering coefficients.[21] The absorption and scattering coefficients of the clay ($\mu_a = 0.014\ mm^{-1}$, $\mu'_s = 0.55\ mm^{-1}$) match reasonable values of skin and/or adipose human tissue. The gantry angle is set as 0°, and the photon field is delivered using a field size of 8×8 cm^2 and source-to-surface distance (SSD) of 100 cm. Unless otherwise specified, the concentration of cQD sheeting used is 0.1 mg/ml in this part.

1. Luminescence uniformity and stability

100 MU is delivered with the static 6 MV and 10 MV, 200–600 MU/min beam to verify the luminescence uniformity and stability of cQD sheeting. This process is repeated three times, and the standard deviation is quantified as measurement uncertainty.

2. Dose-response

To assess dose-response, the relationship between the optical intensity and the delivered dose is evaluated in solid water with cQD sheeting of concentrations of 0, 0.05, and 0.1 mg/ml. The dose rate is set to 600 MU/min for delivered doses of 100, 200, 300, 400, and 500 MU at 6 and 10 MV, respectively. Starting from 100 MU, the monitor units are varied successively by ±3%, ±6%, ±9%, and ±12% for solid water without sheeting and

with 0.1 mg/ml cQD sheeting, respectively, to verify the dose-response sensitivity of cQD sheeting.

3. Comparison of the optical profile and the dose distribution

To verify the consistency between the optical profile and the dose distribution, the EBT3 film is used to measure the 2D dose distribution in the solid water. The film is placed on the surface of solid water, 100 MU is delivered with the static 6 MV, 600 MU/min beam, the optical images w/ and w/o cQD sheeting are obtained under the same conditions, respectively.

4. Analysis of the light intensity and the signal-to-noise ratio

The dose rate dependence of the light intensity and the SNR of cQD sheeting with different concentrations (i.e., 0, 0.05, and 0.1 mg/ml) is explored in this section. A constant dose of 100 MU is delivered to solid water, and the dose rate is set to 200, 300, 400, 500, and 600 MU/min at 6 MV and 10 MV, respectively.

For the second part, the physical anthropomorphic phantom is used to represent the patient's geometry. The gantry angle is set to 0°, the beam field is 6×8 cm^2 at the isocenter, and SSD is 100 cm. The concentration of cQD sheeting used is 0.1 mg/ml.

1. Imaging effect with different radiotherapy materials

To assess the effect of different radiotherapy materials on the optical signal, the cQD sheeting is placed on a bolus, mask sample, and the combination of bolus and mask respectively to observe the influence of cQD sheeting on the quality of the detected signal. Meanwhile, the dependence of optical properties is further discussed by repeating the experiment with three different color shades of Sculpey clay.

2. Imaging effect with ambient light

To suppress the influence of ambient light on light detection, the indoor lighting is turned off before image acquisition in the previous studies. In the section of imaging effect with ambient light, to explore the optical imaging effect of cQD sheeting under the existence of ambient light, red LED is placed on the couch as environment light source, as shown in Figure 10a and the spectrum is shown in Figure 10d. In consideration of the spectral separation, a 420 ± 10 nm (emission peak of cQD) band-pass filter (Limit Optics) is placed behind the lens (6 mm thick and 24 mm diameter). The dose rate is set to 600 MU/min for a delivered dose of 100 MU at 6 MV.

2.3 | Image acquisition and processing

All images in this work are obtained using a tripod-mounted EMCCD camera (Andor iXon ultra-888) with a 40 mm f/1.8 Canon lens. The sensitive detection spectra of the camera as shown in Figure 1b. The relative position between the camera and the beam direction is shown in Figures 2e and f. By comparing SNR with different exposure times, 0.5 s is determined as the optimal exposure time. Background image with the same exposure time is collected after each beam output, and it is subtracted from each frame of images collected during beam output. To eliminate the noise caused by stray radiation, 7×7 median filtering is adopted on each image. To account for pixel-by-pixel differences in light response, dark-field and flat-field correction are used for post-processing of all images.

In order to compare the optical profile and dose distribution, reference points are extracted to correct for the skewed perspective angle of the camera, relative to the plane of the imaged solider water. The reference points are selected according to the four corners of solid water, as performed in previous studies.[22] Using the light field method of calibrating pixel size, a scalable factor of 0.68 mm/pixel is determined.[23]

3 | RESULTS

3.1 | Optical characteristics of cQD sheeting

3.1.1 | Luminescence uniformity and stability

The luminescence uniformity is estimated by the percentage deviation of mean optical intensity in five regions of interest (ROIs) (50×20 pixel) selected from the middle of the radiation field. The analysis on the uniformity of optical emission is used to verify the uniformity of cQD distributed in sheet under our preparation process. Two groups of data at 6 MV and 10 MV are analyzed, as shown in Figures 3a and b, respectively. With the impact of underlying dose profile, the percentage deviation of optical distribution is less than 3.3% within the dose rate range of 200–600 MU/min, which can be proved that the luminescence has good uniformity and the distribution of cQD in the sheeting has suitable uniformity. Luminescence stability is assessed by selecting the average optical intensity in the ROI (50×120 pixels) of 40 frames. As shown in Figure 3c, the standard deviation of the counts per frame is 2.78 (the average intensity is 46.44), and the standard deviation without cQD sheeting is 1.895 (the average optical intensity is 22.973) at 6 MV. Similar results are obtained at 10 MV as shown from Figures 3d.

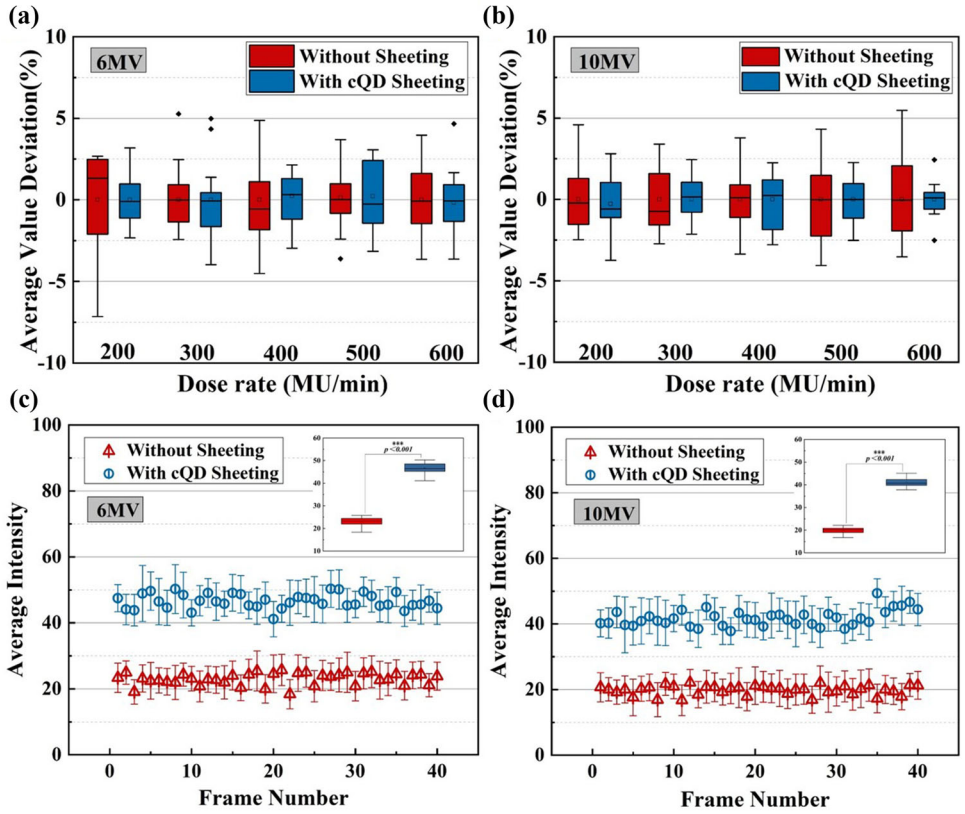

FIGURE 3 (a, b) Average value deviation for five chosen adjacent ROIs of the solid water without sheeting (red) and with cQD sheeting on (blue) at 6 and 10 MV, respectively. (c, d) Average intensity for a ROI chosen around the midpoint of the solid water without sheeting (red) and with cQD sheeting on (blue) at 6 and 10 MV, respectively. The error bar represents the standard deviation of the data obtained from three repeated experiments. The inset shows statistically significant difference in with vs without sheeting

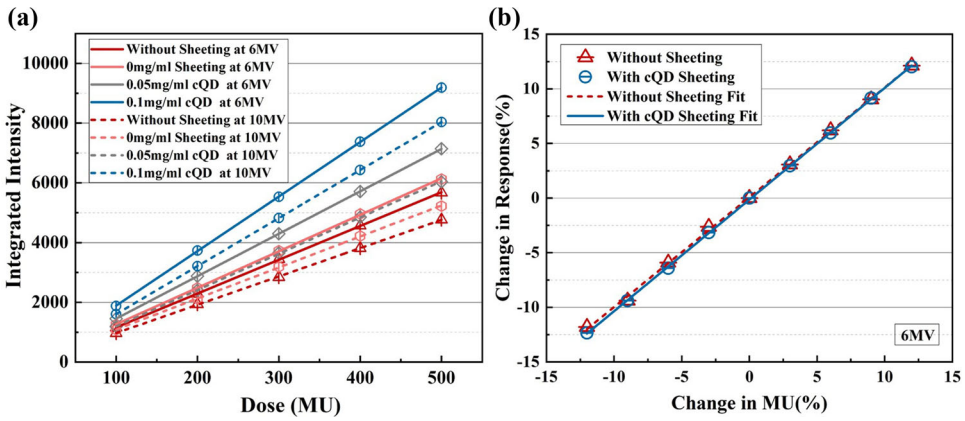

FIGURE 4 (a) Integrated intensities measured for with cQD sheeting of concentrations of 0 mg/ml (grey), 0.05 mg/ml (orange), 0.1 mg/ml (red) and without sheeting (blue) as a function of the MU at 6 MV (full line) and 10 MV (dashed line), respectively. (b) Sensitivity of optical intensity without sheeting (red) and with cQD sheeting on (blue) to small changes in accelerator output with the static 6 MV

3.1.2 | Dose-response

Figures 4a shows the dose-response of luminescence when covered by cQD sheeting with concentrations of 0, 0.05, and 0.1 mg/ml, and with no sheeting under 6 MV and 10 MV beam irradiation. The total optical intensity collected has an excellent linear relationship ($R^2 > 0.99$) with the dose for 6 MV and 10 MV photons. As can be seen from Figure 4b, even for a change of 3% (3 MU) in dose output, optical counts also show a high response sensitivity and linearity within the dose change range of 3–12 MU, no matter with and without the cQD sheets. The R^2 corresponding to the presence and absence of cQD sheeting is 0.9998 and 0.9993 at 6 MV, respectively. The overlap of the two fitting lines reflects the consistency of the response sensitivity of

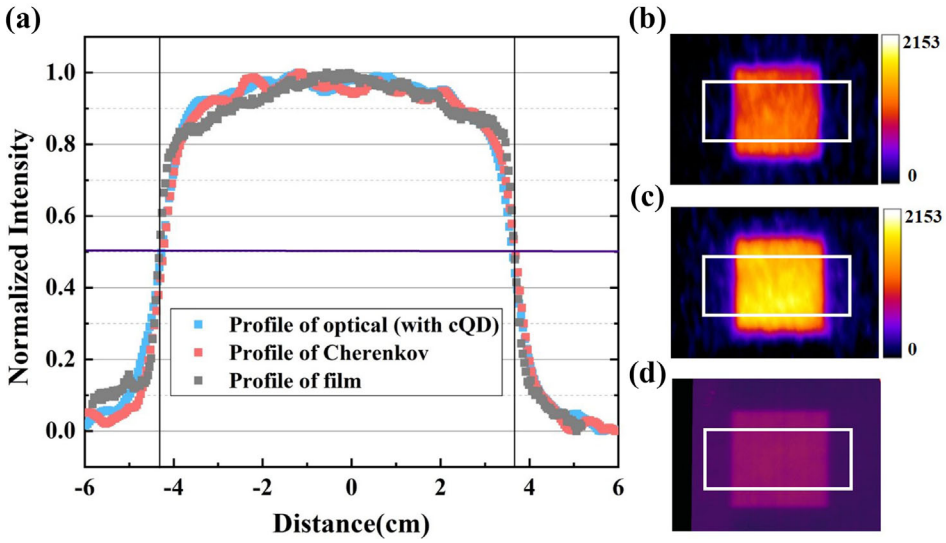

FIGURE 5 (a) Comparison between the 2D profiles of optical imaging and film measurement. (b) 2D profile of optical emission without sheeting. (c) 2D profile of optical emission with cQD sheeting. (d) 2D profile of field from EBT3 film measurement

TABLE 1 Results of beam width measurements with vs without cQD sheeting

Direction	Nominal beam size/cm	Film width/cm	Optical width (without cQD)/cm	Optical width (with cQD)/cm	Error without cQD/mm	Error with cQD/mm
X	8	8	7.91± 0.25	8.07± 0.05	0.9± 2.5	0.7± 0.5
Y	8	8	8.22± 0.17	8.15± 0.12	2.2± 1.7	1.5± 1.2

The number after ± represent the standard deviation of the data obtained from three repeated experiments.

the two optical systems. This indicates that the addition of sheeting changes the dose response of optical intensity, but it still has the same response sensitivity as that without sheeting.

3.1.3 | Comparison of the optical profile and the dose distribution

The perspective transformation is applied to the optical images captured with or without cQD sheeting, and the transformed results are shown in Figures 5b and c. The optical boundaries are determined by the full width at half maximum (FWHM) of the optical image in the lateral direction, as shown in Figures 5a. The irradiated EBT3 film is scanned by a film scanner (EPSON V850 pro) and saved tiff image for analysis (Figure 5d), this location is illustrated in Figure 5a. The results of measurements are summarized numerically in Table 1, listing the width from film measurement and Cherenkov emission analysis with versus without cQD sheeting. The calculation results show that the optical width with or without cQD sheeting is in good agreement with the film width. In the x-direction, the average discrepancy without sheeting between measured and field size is 0.9 mm, while that with cQD sheeting this number is 0.7 mm. In the y-direction, corresponding average discrepancy is 2.2 and 1.5 mm, respectively.

3.1.4 | Analysis of the light intensity and the SNR

To quantify the improvement of image quality after adding cQD sheeting, we choose light intensity and SNR for quantitative analysis. SNR is defined as

$$\mathrm{SNR} = \mathrm{mean}\left(\frac{\mathrm{OPT}(i,\ j) - \mu_{\mathrm{BKG}}}{\sigma_{\mathrm{BKG}}}\right) \quad (1)$$

where OPT(i, j) is the count of pixels (i, j) in the luminescence region $\mathrm{ROI}_{\mathrm{OPT}}$, while μ_{BKG} and σ_{BKG} are the mean count and standard deviation of $\mathrm{ROI}_{\mathrm{BKG}}$ in the background area, respectively. The selection of $\mathrm{ROI}_{\mathrm{OPT}}$ and $\mathrm{ROI}_{\mathrm{BKG}}$ is shown in Figure 6a. The mean OPT(i,j) of $\mathrm{ROI}_{\mathrm{OPT}}$ is defined by the light intensity of the luminescence area to analyze the improvement of SNR through cQD sheeting. Figures 6b and c show the change of SNR accumulated by 1–12 frames of images at 6 and 10 MV, respectively. The SNR is increasing with the increase of cumulative frames (i.e., exposure time). Single-frame images of luminescence from solid water without

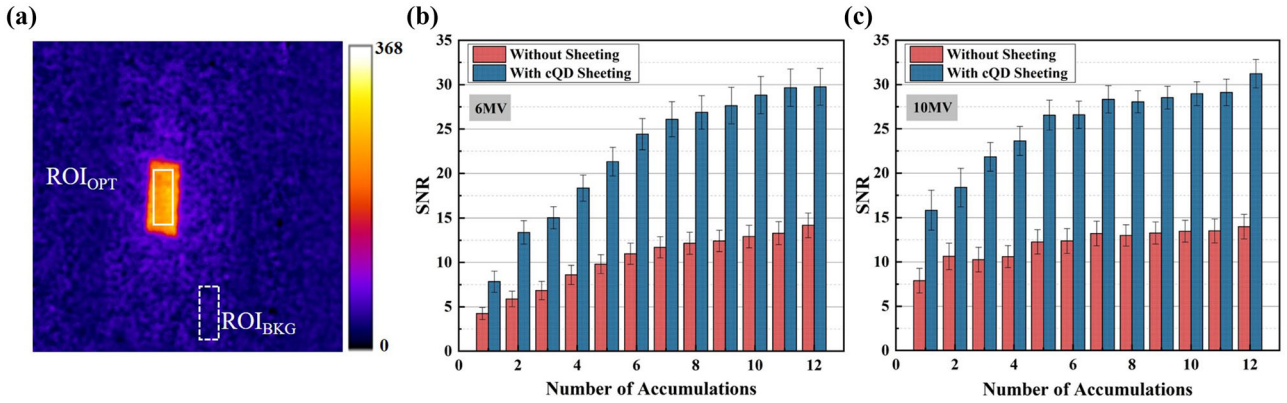

FIGURE 6 (a) Luminescence emission image with luminescence (solid) and background (dashed) ROI used for calculation of SNR. The physical size of the ROI and beam is 5.76 cm × 2.15 cm and 8.0 cm × 8.0 cm, respectively. (b, c) SNR for accumulation of different frame numbers with and without cQD sheeting at 6 and 10 MV, respectively

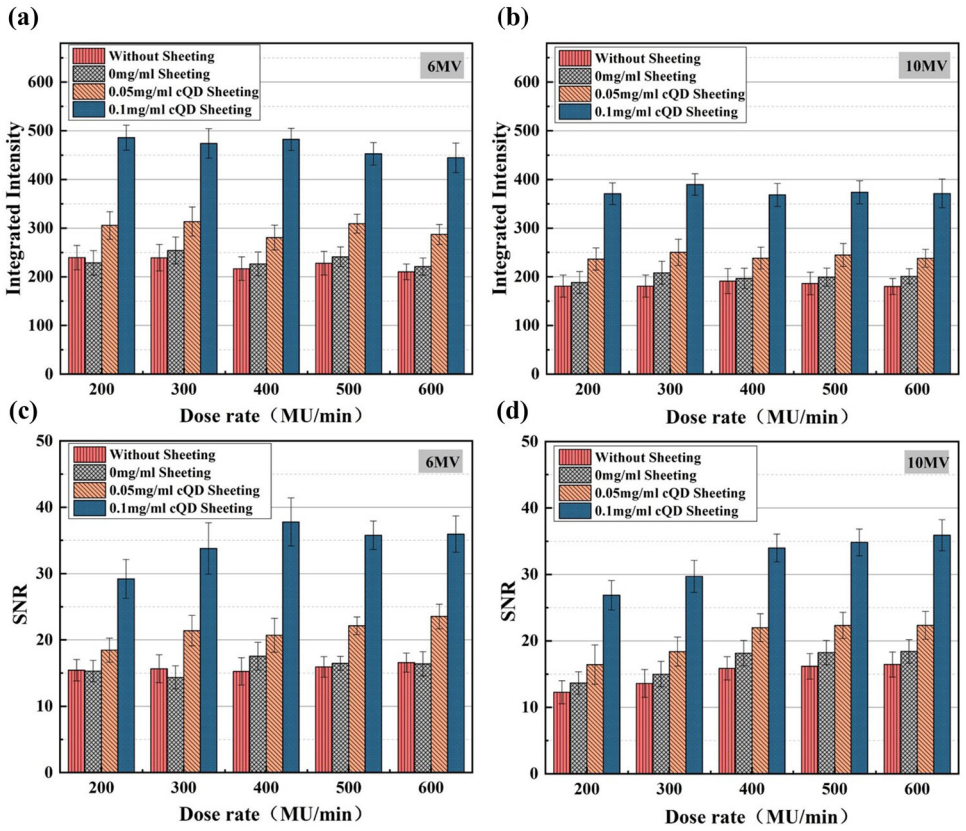

FIGURE 7 (a, b) Integrated intensity I_{OPT} and (c, f) SNR for optical images with cQD sheeting of concentrations of 0 mg/ml (grey), 0.05 mg/ml (orange), 0.1 mg/ml (red) and without sheeting (blue) with the static 6 MV and 10 MV beam, respectively

sheeting and with cQD sheeting is shown in Figure 2c and d. At 6 MV, the SNR accumulated by 12 frames of images with cQD sheeting is about 2.1 times higher than without sheeting, and approximately 2.23 times at 10 MV.

The changes in light intensity of sheeting with different concentrations sheeting are shown in Figures 7a and b. All of them seem to have a good dose-rate stability with or without cQD sheeting. There is no statistically significant difference in light intensity between different dose rates through the use of two-sample *t*-test. For 0.05 mg/ml, the percentage deviations of light intensity for dose rates varying from 100 to 600 MU/min at 6 MV and 10 MV are less than 11.67% and 5.83%, respectively, which are 9.29% and 5.79%, respectively, for 0.1 mg/ml. The changes in SNR of sheeting with different concentrations and without sheeting are shown in Figures 7c and d. For 0.05 mg/ml, the SNR increases by 19.64%~41.85% and 33.92%~38.51% for dose rates

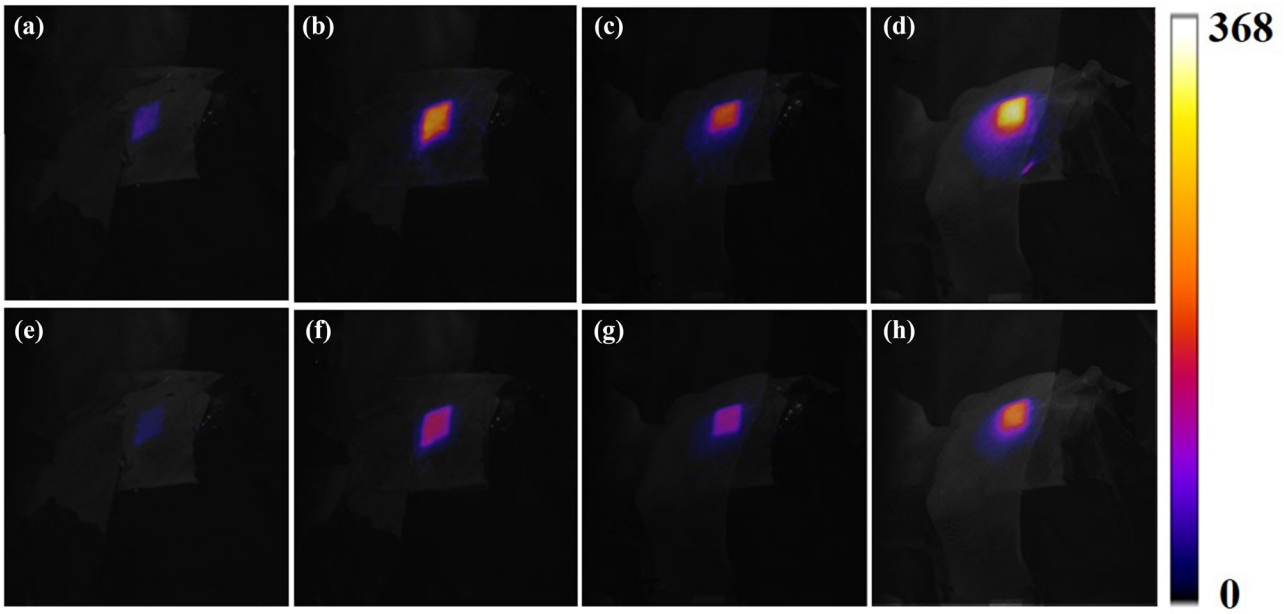

FIGURE 8 The top row (a-d) shows images for tissue-colored clay, transparent bolus, mask samples, and the combination of bolus and mask from treatment with cQD sheeting. The bottom row (e-f) shows images from treatment without sheeting

TABLE 2 Integrated intensity and SNR values for different radiotherapy materials with versus without cQD sheeting

Attachment of phantom	Integrated intensity			SNR		
	Without sheet	With sheet	Delta (%)	Without sheet	With sheet	Delta (%)
Tissue-colored clay	8.56	23.52	174.77	6.96	17.87	156.75
Bolus	126.78	214.57	69.25	82.86	134.87	62.77
Mask	101.74	166.58	63.73	53.13	83.29	56.77
Bolus+ mask	194.81	315.16	61.78	97.6	164.74	68.79

The integrate intensity is units of pixel counts.

varying from 200 to 600 MU/min at 6 and 10 MV, respectively.

3.2 | Imaging effects on the anthropomorphic phantom

3.2.1 | Imaging effects with different radiotherapy materials

The optical distribution image of each material is shown in Figure 8. It can be seen in Table 2 that the average optical intensity increased by about 69.25%, 63.72%, and 61.78%, respectively, after adding the cQD sheeting to bolus, mask sample and the combination of bolus and mask. Corresponding SNR is improved by about 62.78%, 56.77%, and 68.80%, respectively.

Using three different color shades of Sculpey clay with different optical properties, the optical intensity with and without cQD sheeting is imaged (Figure 9). Average intensity images are analyzed in the ROI for each type. As the clay color increases, less Cherenkov photons escape the surface therefore less cQD is excited. Measurements of optical emission from clay3 with sheet are more than 6× greater than that from clay1.

3.2.2 | Imaging effect with ambient light

The imaging with ambient light is shown in Figures 10b and c shows the optical images with the filter. After adding the filter, the SNR of the images obtained with ambient light is improved. Compared with the case without filter, the SNR under red LED with filter is increased by about 98.85% (as shown in Figure 10e).

4 | DISCUSSION

In recent years, Cherenkov imaging has been proposed for dosimetry and monitoring positions of patients during radiotherapy. The low intensity of the Cherenkov

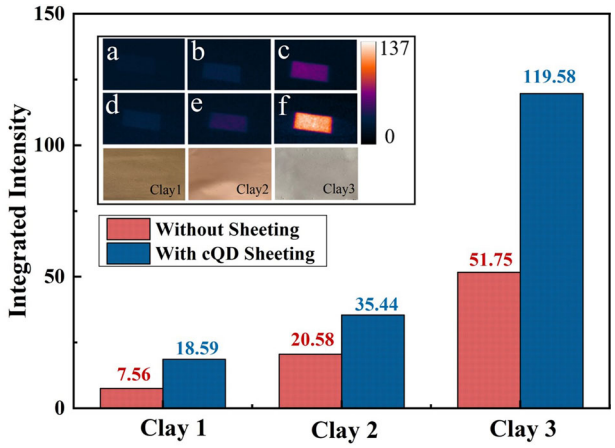

FIGURE 9 Relative intensity for three different tissue-colored clays. The top row (a-c) shows optical images without sheeting, while the bottom row (d-f) shows images with cQD sheeting

emission coupled with the need of ambient room light for patient safety has restricted the wide application of this method. In this study, cQD is utilized to improve Cherenkov image quality, we propose to prepare a cQD sheeting that can be attached to the surface of the skin, to improve the detection efficiency of light intensity and obtain images with high light intensity and SNR for *in*-vivo optical surface dosimetry. Jenkins et al. prepared scintillating sheets by mixing GOS scintillating phosphor powder and a silicone elastomer to realize real-time beam visualization.[24] Compared with this method, the cQD sheeting prepared in our study have the following advantages. The thickness was reduced by about 72%, the reduction of thickness can suppress the perturbation to the radiation beam and the surface dose deposition. CQD is spin coated on the surface of the plastic substrate to ensure that the scintillation material does not directly contact the skin. CQD sheeting is almost transparent and do not block Cherenkov emission from tissues, therefore, it is going to be inherently dependent on the optical properties of the tissue beneath it. When imaging human tissue, the heterogeneity in patient absorbing and scattering properties introduces nonlinearity between Cherenkov emission signal and deposited dose. Monte Carlo simulations estimate that tissue absorption and scattering events can contribute up to 45% variation in the detected light.[25] If the method is further applied to real-time dosimetry, it is necessary to explore the variety of different intra- and inter-patient variability in superficial tissue types during Cherenkov imaging. Hachadorian et al. examined the potential to correct for superficial vasculature using spatial frequency domain imaging to map tissue optical properties for large fields of view,[26] and corrected the Cherenkov intensity by extracting X-ray CT to eliminate the influence of dependence on intrinsic tissue optical properties.[27] Our repeated experiments with three different color shades of Sculpey clay as shown in Figure 9 also show that optical properties of clay affect the optical intensity. Scintillator disks prepared by the Tendler et al provide the potential to eliminate the inherent dependent on tissue optical properties, which also expands our thinking for future dosimetry research.[24]

To characterize the optical properties of the cQD sheeting, luminescence uniformity, stability, and dose-response must be analyzed. Results show that compared with and without cQD sheeting, there is similar luminescence uniformity in the selected ROIs. The total optical intensity collected has an excellent linear relationship ($R^2 > 0.99$) with the dose for 6 and 10 MV photons and the stability of luminescence of cQD does not change in the continuous irradiation with the max dose of 500 MU. It is noteworthy that the light intensity of sheeting with the concentration of 0 mg/ml is also slightly higher than that without sheeting. A possible explanation for this inconsistency might be that transparent colloids have lower optical attenuation coefficients and more Cherenkov photons can be emitted and captured by the camera. In the case of 6 MV, the SNR of one frame with sheeting (7.843) is higher than that of three frames without sheeting (6.839). In other words, when acquiring images with the same SNR, the exposure time required for adding cQD sheeting is about three times shorter than that without it. So, the time resolution of real-time monitoring can be improved while ensuring a high SNR of image.

The boundaries of optical images Figure 5b and c on a solider water are more blurred than those of the radiation field as reported by the EBT3 film Figure 5d. This is expected due to point spread function of the optical system and the scattering of light. If Cherenkov imaging is used as the verification tool for quality assessment before radiotherapy treatment, this blurring is affected by the optical properties of imaging plates with different materials, a less translucent plate could be used in the measurement to reduce the optical scatter diffusion at the edges, as the research of Miao et al.[28] However, in real-time beam visualization during treatment, scattering mainly depends on the tissue characteristics of the patients, the variability associated with lateral scatter in the imaged tissue is a factor to blur the edges of the beam image. Therefore, radiotherapy technicians should carefully and accurately evaluate the light field edge when using this method to monitor the radiation field. Meanwhile, in order to acquire optimal Cherenkov light emission intensity, the downward facing angle of the camera and incident beam direction is set to 45°. The result of film measurement is served as the gold standard for measurement to verify the consistency between the optical profile and the dose distribution. The accuracy of film measurement also can be subject to increased variation depending on the film scanned method. The method of film measurement proposed by Fiandra et al. has been adopted in this work to avoid the measurement error as much as possible.[29]

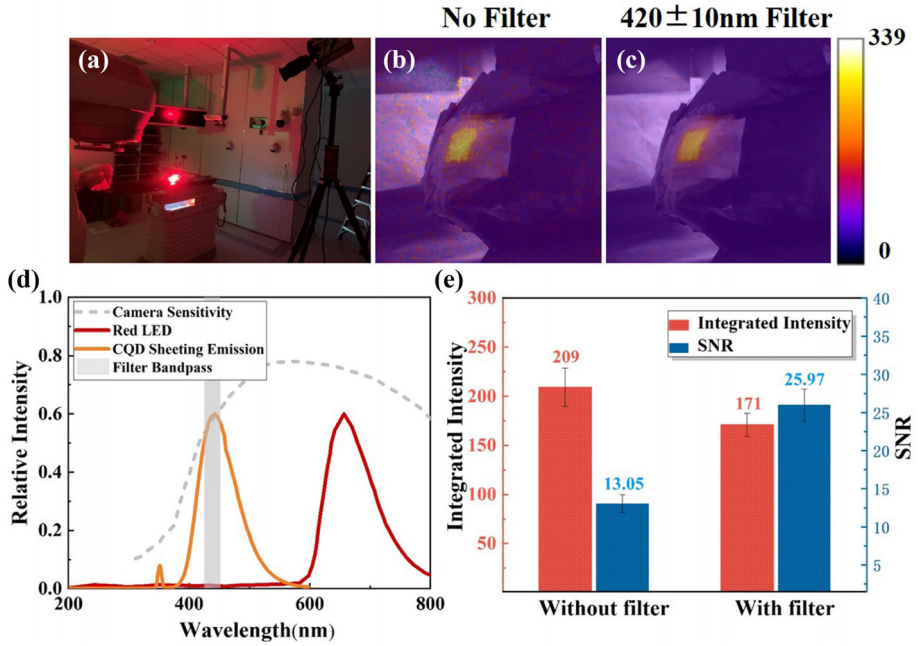

FIGURE 10 (a) The treatment room with the red LED light source. (b) Optical image under red LED ambient light. (c) Optical image under red LED ambient light with filter. (d) Diagram of LED and cQD sheeting emission spectra, camera sensitivity and the filter bandpass. (e) Integrated intensity I_{OPT} and SNR for red LED source considered with and without a 420±10 nm filter

Regarding beam profiles, it has been observed that the inline profile exhibits more blurring in this angle.[22] The profile measurements in y-axis are more subject to skewed perspective angle of the camera, and the oblique viewing angle limits image resolution in the y-direction. This leads to smearing in the interpolation during image transformation, increasing the error in the y-direction. It also occurs in other applications of perspective transformation.[22] This effect could be reduced with the use of a checkerboard pattern to extract more pixel locations of the corners as discrete points to calculate transformation matrix.[28] The depth of field (DOF), type of lens and imaging distance from the object also need to be taken into account to avoid out-of-focus imaging of the beam. When considering quantitatively accurate optical beam profiling, the DOF should be greater than the width of the beam in the direction parallel to the camera viewing direction to avoid out-of-focus imaging of the beam. Through the DOF calculation formula used by Glaser et al.,[30] the DOF of our imaging setup in the first part is 9.27 cm. This imaging geometry would therefore be adequate for imaging the beam delivered during our experiment.

To further explore the imaging effect of the cQD sheeting on different radiotherapy materials, such as bolus, mask sample, and the combination of bolus and mask are used to observe the influence of cQD sheeting on the quality of the detected signal. Light emission from the surface of the different radiotherapy materials with cQD sheeting is all over 60% more than without sheeting. The corresponding SNR is also increased by more than 55%. These results indicate that the cQD sheeting could be applied to different radiotherapy materials attached to the surface of the body, to obtain images with high light intensity and SNR. Future studies will test more irregular surfaces to further explore the performance of surface dosimetry. Finally, in consideration of the optical imaging effect of cQD sheeting under the existence of ambient light, red LED is used as ambient light sources. Through the cQD sheeting, optical images with SNR > 5 can be obtained in the presence of ambient light. After adding a filter, the SNR of the image obtained with ambient light is increased and the intensity of optical capture is reduced using the filter. A large fraction of the ambient light is suppressed by filter while maintaining the most of the optical emission detected by the camera, which is similar with the other studies.[31] There is abundant room for further progress in combining fluorescent materials with different emission spectra with corresponding different filters to make the study more systematic. Meanwhile, all images in this study are obtained using an EMCCD camera with high photon sensitivity. Under this imaging system, the SNR tends to decrease with the decrease of dose rate. This can result from that at lower average dose-rates, time between radiation pulses increases and therefore more background signal is acquired. This will not be an issue if the camera is synchronized to the radiation pulses. Meanwhile, in patient verification, complexities include analyzing fields from diverging beams that are summed from non-rectangular fields on the irregular surface with complicated geometries and different optical properties, so there is an existing deficit in our research to explore the complexity of this method during human radiation

treatments. Future studies will attempt to increase the concentration of cQD in sheeting to acquire images with high signal and SNR, and carry out human imaging experiments further discuss the above issues if available.

5 | CONCLUSION

In this study, we have achieved the improvement of SNR and image quality of optical imaging in surface dosimetry by preparing a flexible cQD sheeting which is non-toxic and can be directly attached to the surface of human body. The luminescence uniformity, stability and dose-response of cQD sheeting is characterized through optical imaging experiments. The imaging on the phantom verified that cQD sheeting could be applied to different radiotherapy materials to obtain images with a high light intensity and SNR. The cQD sheeting allows optical images with SNR $>$ 5 to be obtained in the presence of ambient light and can be improved by the combination with a band-pass filter. This approach provides novel insights into optical imaging for real-time beam visualization and can be utilized as a versatile beam monitoring tool in radiotherapy.

ACKNOWLEDGMENTS

This study was supported by the National Natural Science Foundation of China [Grant No. 12005102, No. 12075120], the Natural Science Foundation of Jiangsu Province [Grant No. BK20220132], the Primary Research and Development Plan of Jiangsu Province [Grant No. BE2019002-3], and the Foundation of Graduate Innovation Center in NUAA [Grant No. xcxjh20210623].

CONFLICT OF INTEREST

The authors have no relevant conflicts of interest to disclose.

REFERENCES

1. Schaue D, Mcbride WH. Opportunities and challenges of radiotherapy for treating cancer. *Nat Rev Clin Oncol*. 2015;12(9):527-540. https://doi.org/10.1038/nrclinonc.2015.120
2. Camma C, Giunta M, Fiorica F, Pagliaro L, Craxi A, Cottone M. Preoperative radiotherapy for resectable rectal cancer: a meta-analysis. *J Am Med Assoc*. 2000;284(8):1008-1015. https://doi.org/10.1001/jama.284.8.1008
3. Van Herk M. Errors and margins in radiotherapy. *Semin Radiat Oncol*. 2004;14(1):52-64. https://doi.org/10.1053/j.semradonc.2003.10.003
4. Shiau AC, Lai PL, Liang JA, Shueng PW, Chen WL, Kuan WP. Dosimetric verification of surface and superficial doses for head and neck IMRT with different PTV shrinkage margins. *Med Phys*. 2011;38(3):1435-1443. https://doi.org/10.1118/1.3553406
5. Zhuang AH, Olch AJ. Validation of OSLD and a treatment planning system for surface dose determination in IMRT treatments. *Med Phys*. 2014;41(8). https://doi.org/10.1118/1.4890795
6. Warkentin B, Steciw S, Rathee S, Fallone BG. Dosimetric IMRT verification with a flat-panel EPID. *Med Phys*. 2003;30(12):3143-3155. https://doi.org/10.1118/1.1625440
7. Äerenkov PA. Visible radiation produced by electrons moving in a medium with velocities exceeding that of light. *Phys Rev*. 1937;52(4):378-379. https://doi.org/10.1103/PhysRev.52.378
8. Zhang R, Fox CJ, Glaser AK, Gladstone DJ, Pogue BW. Superficial dosimetry imaging of Čerenkov emission in electron beam radiotherapy of phantoms. *Phys Med Biol*. 2013;58(16):5477-5493. https://doi.org/10.1088/0031-9155/58/16/5477
9. Shu D, Tang X, Geng C, Gong C, Chen D. Determination of the relationship between dose deposition and Cerenkov photons in homogeneous and heterogeneous phantoms during radiotherapy using Monte Carlo method. *J Radioanal Nucl Chem*. 2016;308(1):187-193. https://doi.org/10.1007/s10967-015-4316-x
10. Ai Y, Tang X, Shu D, et al. Measurement of dose in radionuclide therapy by using Cerenkov radiation. *Australas Phys Eng Sci Med*. 2017;40(3):695-705. https://doi.org/10.1007/s13246-017-0579-6
11. Jarvis LA, Zhang R, Gladstone DJ, et al. Cherenkov video imaging allows for the first visualization of radiation therapy in real time. *Int J Radiat Oncol Biol Phys*. 2014;89(3):615-622. https://doi.org/10.1016/j.ijrobp.2014.01.046
12. Hachadorian R, Farwell JC, Bruza P, et al. Verification of field match lines in whole breast radiation therapy using Cherenkov imaging. *Radiother Oncol*. 2021;160:90-96. https://doi.org/10.1016/j.radonc.2021.04.013
13. Alexander DA, Tendler II, Bruza P, et al. Assessment of imaging Cherenkov and scintillation signals in head and neck radiotherapy. *Phys Med Biol*. 2019;64(14). https://doi.org/10.1088/1361-6560/ab25a3
14. Xie Y, Petroccia H, Maity A, et al. Cherenkov imaging for total skin electron therapy (TSET). *Med Phys*. 2020;47(1):201-212. https://doi.org/10.1002/mp.13881
15. Andreozzi JM, Zhang R, Gladstone DJ, et al. Cherenkov imaging method for rapid optimization of clinical treatment geometry in total skin electron beam therapy. *Med Phys*. 2016;43(2):993-1002. https://doi.org/10.1118/1.4939880
16. Geng CR, Ai Y, Tang XB, et al. Quantum dots enhanced Cerenkov luminescence imaging. *Nucl Sci Tech*. 2019;30(5):3-7. https://doi.org/10.1007/s41365-019-0599-x
17. Zhang R, Glaser AK, Davis SC, Gladstone DJ, Pogue BW. Time-gated Cherenkov emission spectroscopy from linear accelerator irradiation of tissue phantoms. *Biomed Opt BIOMED 2012*. 2012;37(7):1193-1195. https://doi.org/10.1364/biomed.2012.bw4b.5
18. Ashraf MR, Bruza P, Krishnaswamy V, Gladstone DJ, Pogue BW. Technical note: time-gating to medical linear accelerator pulses: stray radiation detector. *Med Phys*. 2019;46(2):1044-1048. https://doi.org/10.1002/mp.13311
19. Goddu SM, Westphal GT, Sun B, et al. Synchronized high-speed scintillation imaging of proton beams, generated by a gantry-mounted synchrocyclotron, on a pulse-by-pulse basis. *Med Phys*. 2022;49(9):6209-6220. https://doi.org/10.1002/mp.15826
20. Azam N, Najabat Ali M, Javaid Khan T. Carbon quantum dots for biomedical applications: review and analysis. *Front Mater*. 2021;8(August):1-21. https://doi.org/10.3389/fmats.2021.700403
21. Ahmed SR, Jia JM, Bruza P, et al. Radiotherapy-induced Cherenkov luminescence imaging in a human body phantom. *J Biomed Opt*. 2018;23(03):1. https://doi.org/10.1117/1.jbo.23.3.030504
22. Alexander DA, Zhang R, Brůža P, Pogue BW, Gladstone DJ. Scintillation imaging as a high-resolution, remote, versatile 2D detection system for MR-linac quality assurance. *Med Phys*. 2020;47(9):3861-3869. https://doi.org/10.1002/mp.14353
23. Black PJ, Velten C, Wang YF, Na YH, Wuu CS. An investigation of clinical treatment field delivery verification using cherenkov imaging: iMRT positioning shifts and field matching. *Med Phys*. 2019;46(1):302-317. https://doi.org/10.1002/mp.13250

24. Jenkins CH, Naczynski DJ, Yu SJS, Xing L. Monitoring external beam radiotherapy using real-time beam visualization. *Med Phys*. 2015;42(1):5-13. https://doi.org/10.1118/1.4901255
25. Zhang R, Glaser AK, Andreozzi J, et al. Beam and tissue factors affecting Cherenkov image intensity for quantitative entrance and exit dosimetry on human tissue. *J Biophotonics*. 2017;10(5):645-656. https://doi.org/10.1002/jbio.201500344
26. Hachadorian R, Bruza P, Jermyn M, et al. Correcting Cherenkov light attenuation in tissue using spatial frequency domain imaging for quantitative surface dosimetry during whole breast radiation therapy. *J Biomed Opt*. 2018;24(07). https://doi.org/10.1117/1.jbo.24.7.071609
27. Hachadorian RL, Bruza P, Jermyn M, Gladstone DJ, Pogue BW, Jarvis LA. Imaging radiation dose in breast radiotherapy by X-ray CT calibration of Cherenkov light. *Nat Commun*. 2020;11(1):1-9. https://doi.org/10.1038/s41467-020-16031-z
28. Miao T, Bruza P, Pogue BW, et al. Cherenkov imaging for linac beam shape analysis as a remote electronic quality assessment verification tool. *Med Phys*. 2019;46(2):811-821. https://doi.org/10.1002/mp.13303
29. Fiandra C, Ricardi U, Ragona R, et al. Clinical use of EBT model Gafchromic™ film in radiotherapy. *Med Phys*. 2006;33(11):4314-4319. https://doi.org/10.1118/1.2362876
30. Glaser AK, Davis SC, Voigt WHA, Zhang R, Pogue BW, Gladstone DJ. Projection imaging of photon beams using Čerenkov-excited fluorescence. *Phys Med Biol*. 2013;58(3):601-619. https://doi.org/10.1088/0031-9155/58/3/601
31. Rahman M, Bruza P, Hachadorian R, et al. Optimization of in vivo Cherenkov imaging dosimetry via spectral choices for ambient background lights and filtering. *J Biomed Opt*. 2021;26(10):1-13. https://doi.org/10.1117/1.jbo.26.10.106003

How to cite this article: Di X, Geng C, Guo C, et al. Enhanced Cherenkov imaging for real-time beam visualization by applying a novel carbon quantum dot sheeting in radiotherapy. *Med Phys*. 2023;50:1215–1227. https://doi.org/10.1002/mp.16121